Free-Electron X-Ray Laser Measurements of Collisional-Damped Plasmons in Isochorically Heated Warm Dense Matter

P. Sperling,[1,2] E. J. Gamboa,[1] H. J. Lee,[1] H. K. Chung,[3] E. Galtier,[1] Y. Omarbakiyeva,[2,4] H. Reinholz,[2,5] G. Röpke,[2] U. Zastrau,[6] J. Hastings,[1] L. B. Fletcher,[1] and S. H. Glenzer[1]

[1]*SLAC National Accelerator Laboratory, 2575 Sand Hill Road, MS 72 Menlo Park, California 94025, USA*

[2]*Institut für Physik, Universität Rostock, 18051 Rostock, Germany*

[3]*Nuclear Data Section, Division of Physical and Chemical Sciences, International Atomic Energy Agency, A-1400 Vienna, Austria*

[4]*International IT University, 050040 Almaty, Kazakhstan*

[5]*University of Western Australia, WA 6009 Crawley, Australia*

[6]*European XFEL, Albert-Einstein-Ring 19, 22761 Hamburg, Germany*

(Received 7 April 2015; published 9 September 2015)

We present the first highly resolved measurements of the plasmon spectrum in an ultrafast heated solid. Multi-keV x-ray photons from the Linac Coherent Light Source have been focused to one micrometer diameter focal spots producing solid density aluminum plasmas with a known electron density of $n_e = 1.8 \times 10^{23}$ cm^{-3}. Detailed balance is observed through the intensity ratio of up- and down-shifted plasmons in x-ray forward scattering spectra measuring the electron temperature. The plasmon damping is treated by electron-ion collision models beyond the Born approximation to determine the electrical conductivity of warm dense aluminum.

DOI: 10.1103/PhysRevLett.115.115001 PACS numbers: 52.25.Os, 52.35.Fp, 52.50.Jm, 78.70.Ck

With the advent of the Linac Coherent Light Source (LCLS) [1] and the commissioning of the Matter in Extreme Conditions (MEC) instrument [2], a record peak brightness x-ray beam has become available to study the physical properties of states of matter at high energy density. In the simplest geometry, LCLS delivers 10^{12} multi-keV x-ray photons at 120 Hz in 25 fs-long pulses that are focused to micron-sized focal spots heating solid targets homogeneously and isochorically to temperatures in excess of 1 eV. The highly directional x-ray laser beam provides record peak brightness with a narrow bandwidth, $\Delta E/E = 10^{-4}$, allowing spectrally resolved x-ray Thomson scattering experiments [3] with unprecedented signal-to-noise, spectral, and wave number resolution. Combined with a suite of optical and x-ray diagnostics, MEC thus allows high-precision measurements of the electronic response of matter, particularly in the warm dense matter (WDM) regime [4].

Accurate models of WDM are important for simulations in planetary physics, e.g., for the study of planetary interiors [4–6] or for simulations of inertial confinement fusion implosions [7–9]. The latter requires knowledge of the electrical conductivity in the WDM regime for simulations of the Rayleigh-Taylor instability growth [10] and to accurately model the assembly of thermonuclear fuel.

Previous measurements of the electrical conductivity, especially the static conductivity, were performed on compressed [11–14] and uncompressed matter [15–23]. In these studies, the lack of accurate plasma characterization techniques in the transient WDM regime have made comparisons and critical experimental tests of conductivity calculations challenging. On the one hand, theoretical estimates [24–28] and simulations [29,30] of the conductivity exist and are widely used. On the other hand, experiments have shown order-of-magnitude discrepancies between measurements and calculations [13,19,20]. Predictions of non-Drude conductivities and non-Born collisions have been performed in recent studies [31–35] and await testing with accurate measurements. Consequently, it is important to provide accurate conductivity measurements with simultaneous and independent characterization of densities and temperatures.

In this Letter, we demonstrate highly accurate measurements of the plasmon x-ray scattering spectrum. Our data yield plasmon frequency, damping, and electron temperature. These precision measurements of the longitudinal electron plasma (Langmuir) oscillations, enabled by the ultra bright LCLS x-ray beam, provide unprecedented data with resolution and noise levels well beyond the accuracy obtained from previous experiments utilizing laser-driven x-ray sources [3,36] and thus allow us to infer the dynamical electrical conductivity, σ. Here the density of ultrafast isochorically heated aluminum is known *a priori* [37,38] and the temperature is inferred from first principles using the detailed balance relation [39]. The comparison with theoretical predictions confirms that the plasmon spectrum is sensitive to frequency-dependent electron-ion collision processes which are related to the electrical conductivity. By taking into account strong collisions and dynamical screening [31,40], collisions are treated beyond the Born approximation. We find that this theory establishes agreement with our experimental observations near the plasmon resonance frequency. The collision

frequency ν found in this way is complex and frequency dependent, in contrast to the collision frequency evaluated within the relaxation time approximation [24]. It determines the conductivity via the generalized Drude expression $\sigma(\Delta\omega) = \varepsilon_0\omega_{\mathrm{pl},e}^2/[\nu(\Delta\omega) - i\Delta\omega]$ [31] as a function of frequency shift $\Delta\omega = \omega_f - \omega_i$ between initial and final electrical field frequency.

The experiment has measured the frequency and angularly resolved x-ray scattering spectra of plasmons in isochorically heated aluminum. We utilize 50 μm thick foils that were simultaneously heated and probed [41] with the ultrafast free-electron x-ray laser beam at LCLS [2,42], cf. Fig. 1. The x-ray energy of $E_{\mathrm{LCLS}} = \hbar\omega_{\mathrm{LCLS}} = 7.98$ keV was chosen so that the attenuation length matched the thickness of the foils, leading to isochoric x-ray heating by photoabsorption. We varied the heating by setting the x-ray focal spot (FWHM) to either 1 or 10 μm through the use of compound beryllium refractive lenses [43]. After the 25 fs (FWHM) pulse thermal equilibrium has been established, cf. Fig. 1(b).

To avoid distortion of the plasmon spectra with spectral noise from x-ray amplification [47], the LCLS was operated in the high-resolution seeded mode [48]. Further, adjustable forward scattering spectrometer provides measurements at wave numbers between $k = 0.35$ Å^{-1} and $k = 2.1$ Å^{-1}. The small source size and the focusing of the LCLS beam leads to an extremely small uncertainty of $\delta\theta = 0.3°$ and $\delta k = 0.02$ Å^{-1} [47].

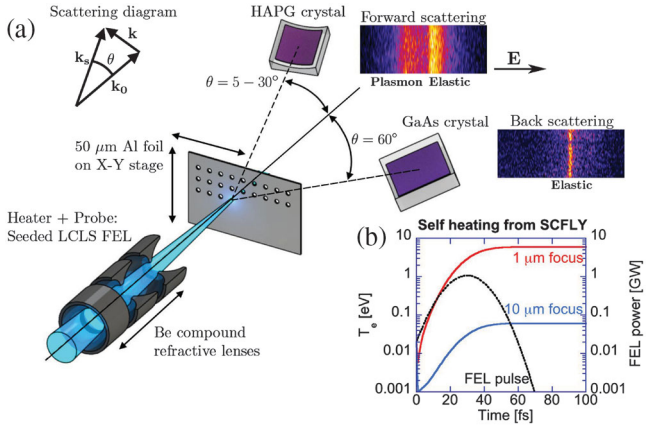

FIG. 1 (color). (a) Schematic of the experimental setup and raw spectra. The seeded LCLS beam at 7.98 keV, 0.1 mJ energy of x rays in a 0.25% bandwidth, and duration of 25 fs (FWHM) containing $\approx 7 \times 10^{10}$ photons, is focused onto a 50 μm thick aluminum foil. The forward scattering spectrometer measures plasmons at scattering angles of $5° < \theta < 30°$ by a Highly Annealed Pyrolytic Graphite (HAPG) crystal in a von Hámos configuration [44] whereas the back scattering spectrometer for scattering angles of 60° provides a highly resolved measure of the source function using a GaAs crystal [45]. (b) Pulse shape and calculated electron temperature as a function of time from the collisional-radiative code SCFLY [46] using focal spot sizes of 1 μm (10 μm) predicting final temperatures of 5.95 eV (0.06 eV).

The total scattering spectrum depends on the dynamic structure factor with contributions from all electrons, usually described via the Chihara formula [3]. For inelastic plasmon scattering we only consider the contributions of free (delocalized) electrons, whose spectrum is sensitive to the plasma conditions. During the scattering process, x rays can either gain or lose energy close to the plasmon resonance frequency ω_{res}, $\Delta\omega_{\mathrm{res}} = |\omega_{\mathrm{LCLS}} \pm \omega_{\mathrm{res}}|$. This leads to a pair of up- and down-shifted peaks, whose relative intensity is determined by the electron temperature T_e via the detailed balance relation $S_{\mathrm{ee}}^0(k,\Delta\omega_{\mathrm{res}})/S_{\mathrm{ee}}^0(-k,-\Delta\omega_{\mathrm{res}}) = \exp[-\hbar\Delta\omega_{\mathrm{res}}/(k_B T_e)]$ [3]. S_{ee}^0 is the dynamic structure factor of free electrons.

Figure 2(a) shows the experimental Thomson scattering data from 2000 shots with a 1 μm focal spot size. Also shown is the instrument function extracted from the spectral comparison of the forward and backward scattering spectrometers (see Fig. 1), deconvolved data, and various theoretical calculations. The data indicate an elastic scattering peak at the energy of the incident LCLS x-ray beam together with a strong plasmon resonance that is downshifted in energy by $\Delta E_{\mathrm{res}} = \hbar\Delta\omega_{\mathrm{res}} = 19$ eV. Because of the high signal-to-noise ratio and accurate x-ray source monitoring we are also able to resolve the up-shifted plasmon on the blue wing at $E = 7999$ eV. Detailed balance determines the temperature to $T_e = (6 \pm 0.5)$ eV. The error bar was calculated from the least square method that applies a 5% deviation between calculated and measured up-shifted plasmon.

Figure 2(b) shows the up-shifted plasmon and calculations which confirm the electron temperature of $T_e = 6$ eV ($T_e = 0.2$ eV) at the end of the heating process with the 1 μm (10 μm) focus [51]. The 6 eV best fit temperature agrees with SCFLY calculations, cf. Fig. 1(b).

Figure 2(a) compares measured and deconvolved spectra with calculations that take into account collisional damping using different approximations. For the calculations, we use $T_e = 6$ eV and an ionization degree of $Z_f = 3$ which yields electron densities of $n_e = 1.8 \times 10^{23}$ cm^{-3}. This result is consistent with SCFLY [46] and COMPTRA04 [28] calculations. The random-phase approximation (RPA) neglects collisions [55]. Collisional damping is considered via the collision frequency ν within the MA [49,50] that in each case includes also local-field corrections [40]. In general, the collision frequency is complex and frequency dependent.

The comparison of the scattering data with calculations shows that a frequency-dependent particle-particle collision operator [51] fits the experiment (best fit). Although some discrepancies between data and theoretical spectra exist, we find that the Gould-DeWitt theory (GDW) $\nu^{\mathrm{GDW}}(\Delta\omega) = \nu^{\mathrm{Born}} + (\nu^{\mathrm{LB}} - \nu^{\mathrm{Born}}) + (\nu^{\mathrm{TM}} - \nu^{\mathrm{Born}})$ approximates the averaged energy shift and the low-energy shift behavior of the plasmon. This approach takes into account weak collisions via the Born approximation ν^{Born}, strong collisions in the T-matrix approximation ν^{TM} [31], and dynamic

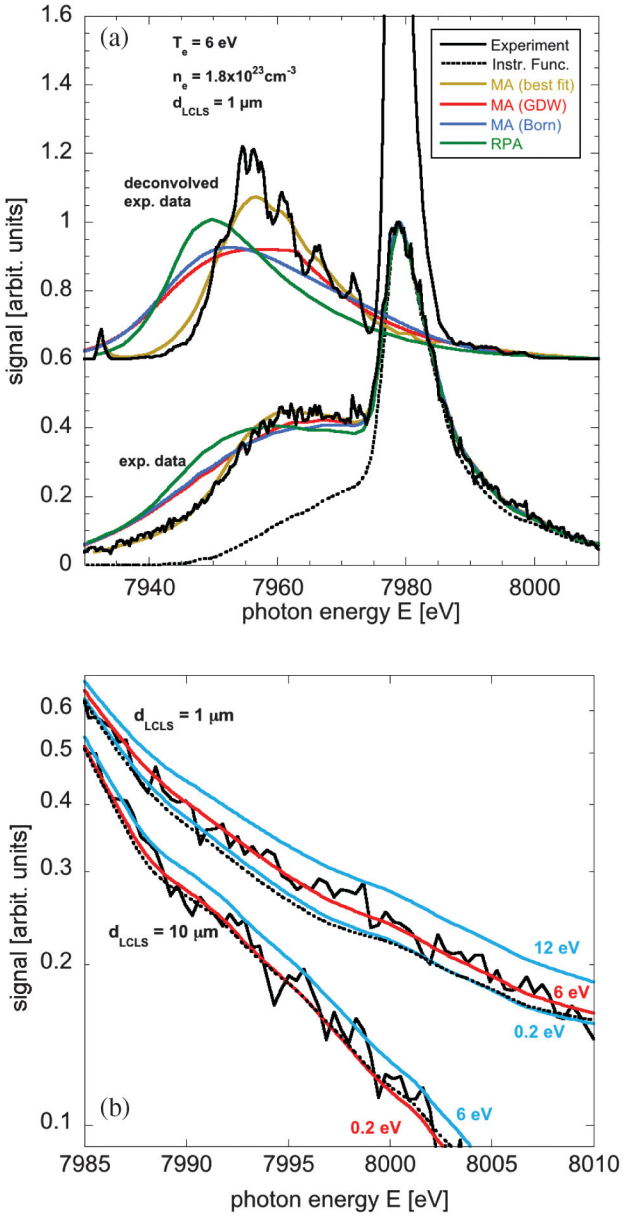

FIG. 2 (color). (a) Measured and deconvolved scattering spectra (solid black) and instrument function (broken black) at an angle of $\theta = 24°$ for a focal spot size of 1 μm. The fit calculations use RPA (green) or the Mermin approach (MA) [40,49,50] with frequency-dependent collision frequencies from best fit (gold), GDW (red), and Born (blue) approximation. The deconvolved data represent the scattering spectra after the subtraction of the instrument function and are offset by 0.6 for clarity. (b) Blue wing of the experimental x-ray scattering spectra (black) for a focal spot size of 1 (offset by 0.1 for clarity) and 10 μm and calculations using MA (GDW, colored) for different free-electron temperatures T_e.

screening via the Lenard-Balescu collision frequency, ν^{LB} [31]. These calculations use Coulomb potentials for electron-ion interactions and neglect ionic structure correlations, i.e., the static ion-ion structure factor $S_{\mathrm{ii}} = 1$.

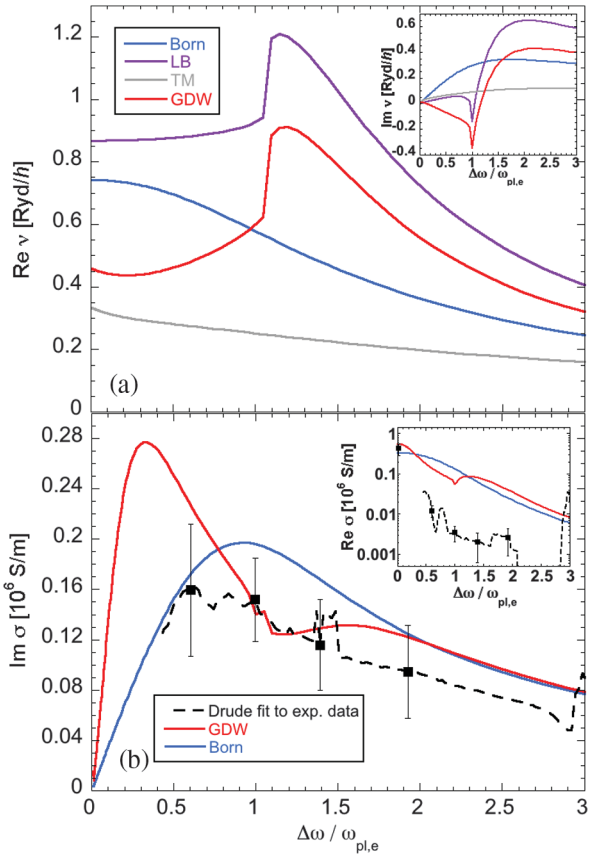

FIG. 3 (color). Calculations of the real and imaginary part of the (a) collision frequency and the (b) electrical conductivity as a function of the frequency shift per plasma frequency $\hbar\omega_{\mathrm{pl},e} = 15.75$ eV at an electron temperature of $T_e = 6$ eV. (a) The collision frequency in the GDW approach is shown in red, and its contributions are Born (blue), Lenard-Balescu (LB, dynamic screening) (purple), and the T-matrix approximation (TM, strong collisions) (gray). (b) Electrical conductivities derived from the generalized Drude expression using the frequency-dependent experimental data extracted (broken line, selected black points for estimation of the experimental error), GDW (red), and Born (blue) collision frequency. The functional dependence of the experimental conductivity is determined by the Drude theory.

Figure 3(a) shows the collision frequency calculated for the conditions of the experiment. The real part of the collision frequency accounts for absorption and the imaginary part for a phase shift of the electrical field, both caused by collisions in the responding plasma. In contrast to the Born approximation, the real part of the GDW approximation shows a sharp maximum near $\omega_{\mathrm{pl},e}$. In addition, GDW yields a negative imaginary part consistent with the best fit results [51]. This property has also been seen in simulations [56]. For our conditions we find that both features are induced by dynamical screening of the electron-ion system describing the influence of collective effects, e.g., plasma oscillations, on the interaction of the plasma with electrical fields. Collective effects lead to additional damping and a shift of the electrical field phase.

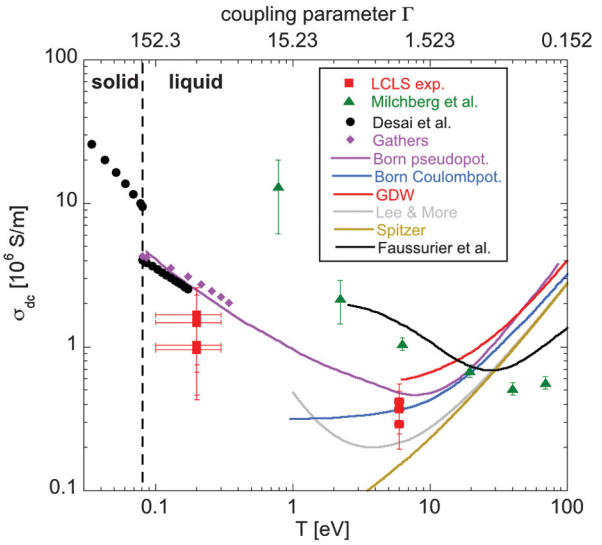

FIG. 4 (color). dc conductivity as a function of the temperature for a density of 2.7 g/cm^3 and an ionization degree of $Z_f = 3$. Extracted results of this work (red squares), experimental results of Desai *et al.* [15] (black dots), Gathers [18] (violet rhombus), and Milchberg *et al.* [20] (green triangles) as well as the theoretical models of Lee and More [24] (gray), Spitzer *et al.* [57] (gold), Faussurier and Blancard [29] (black), GDW [31] (red), and Born [58] (blue) are indicated (screened Coulomb interaction, no ion-ion correlation). To study the influence of the ion-ion structure factor and a pseudopotential [61], the dc conductivity with the corresponding Born collision frequency (Born improved, violet) is also shown.

Figure 3(b) shows the complex electrical conductivity from the generalized Drude expression inferred from the experimental data [51], GDW, and Born collision frequencies. The dc conductivity $\sigma_{\mathrm{dc}} = \sigma(\Delta\omega \to 0)$ is determined from the data extracted collision frequency [51] leveling off to a constant value for $\Delta\omega/\omega_{\mathrm{pl},e} = 0$. In comparison to the Born approximation, GDW shows better agreement with the imaginary part of the experiment near the plasma frequency $\omega_{\mathrm{pl},e}$, implying the relevance of a consistent treatment of collective plasma effects.

Figure 4 shows the dc conductivity of this work, the experiments of Desai *et al.* [15], Gathers [18], and Milchberg *et al.* [20], and theoretical models of Lee and More [24], Spitzer *et al.* [57], Faussurier and Blancard [29], and our theories [25,58]. Within the Lee and More and Spitzer model the Coulomb logarithm of Ref. [59] was used. The dc conductivity agrees in the warm dense matter regime with the Born [58] model assuming screened Coulomb interactions and no ion-ion correlations. Furthermore, our improved Born model [51] reproduces the experimental values in the warm dense matter regime as well as near the melting point. This model applies ion-ion structure factors from classical-map hypernetted chain calculations [60] and temperature dependent pseudopotentials [61] containing Pauli blocking by core electrons.

For aluminum at $T_e = (0.2 \pm 0.1)$ eV, we find $(1.3 \pm 0.7) \times 10^6$ S/m. This value is slightly lower than previous measurements by Desai *et al.*, 2.4×10^6 S/m [15]. Note, we studied isochorically heated aluminum whereas Desai *et al.* and Gathers apply a density dependent correction to account for a heated expanding aluminum liquid. Within the error bars, our result $(0.36 \pm 0.12) \times 10^6$ S/m at $T_e = (6.0 \pm 0.5)$ eV is in agreement with our calculations using the Born approximation 0.37×10^6 S/m and the Born approximation applying a pseudopotential and ion-ion structure factor resulting in 0.46×10^6 S/m. It is smaller than our calculations using the GDW [31,56], 0.59×10^6 S/m, and larger than the model of Lee and More [24], 0.22×10^6 S/m.

In contrast to our results at $T_e = 6$ eV, previous measurements by Milchberg *et al.* [20] show higher conductivity values of 1.053×10^6 S/m. To explain the results of Ref. [20], the following works [27,62] have suggested corrections to the temperature.

In conclusion, we successfully observed highly resolved plasmons by x-ray Thomson scattering in warm dense aluminum isochorically heated and probed with the seeded LCLS beam. We obtain down- and up-shifted plasmons that provide an accurate measurement of the electron temperature. Our measured line profile allows us to extract the complex dynamical conductivity. Using standard relations, we also infer the dc conductivity. Compared to our quantum statistical theory, the imaginary part of the dynamical conductivity agrees quite well but discrepancies persist for the real part possibly indicating a lower electron density in warm dense matter. Taking into account ionic structure correlations and Pauli blocking, our Born model reproduces our inferred dc conductivities in the warm dense matter and near the melting point. It will be important to continue investigating the conductivity in experiments with various temperatures and elements, but also to improve the theoretical approaches to explain the measured data.

We like to thank K. Plagemann, R. Redmer, and H. Rüter for helpful discussions and R. Bredow for providing ion-ion structure factors from CHNC calculations. This work was performed at the MEC instrument of LCLS, supported by the DOE Office of Science, Fusion Energy Science under Contract No. SF00515. The work was supported by the DOE Office of Science, Fusion Energy Science under FWP 100182 and the DFG within the SFB 652. The work was further supported by a Laboratory Directed Research and Development grant, the Alexander von Humboldt Foundation, and the Volkswagen Foundation.

[1] Y. Ding, A. Brachmann, F.-J. Decker, D. Dowell, P. Emma, J. Frisch, S. Gilevich, G. Hays, P. Hering, Z. Huang, R. Iverson, H. Loos, A. Miahnahri, H.-D. Nuhn, D. Ratner, J. Turner, J. Welch, W. White, and J. Wu, Phys. Rev. Lett. **102**, 254801 (2009).

[2] L. B. Fletcher *et al.*, Nat. Photonics **9**, 274 (2015).
[3] S. H. Glenzer and R. Redmer, Rev. Mod. Phys. **81**, 1625 (2009).
[4] R. P. Drake, Phys. Plasmas **16**, 055501 (2009).
[5] B. A. Remington, Plasma Phys. Controlled Fusion **47**, A191 (2005).
[6] J. J. Fortney, S. H. Glenzer, M. Koenig, B. Militzer, D. Saumon, and D. Valencia, Phys. Plasmas **16**, 041003 (2009).
[7] S. H. Glenzer *et al.*, Science **327**, 1228 (2010).
[8] J. D. Lindl, P. Amendt, R. L. Berger, S. G. Glendinning, S. H. Glenzer, S. W. Haan, R. L. Kauffman, O. L. Landen, and L. J. Suter, Phys. Plasmas **11**, 339 (2004).
[9] O. A. Hurricane *et al.*, Nature (London) **506**, 343 (2014).
[10] B. Hammel, S. Haan, D. Clark, M. Edwards, S. Langer, M. Marinak, M. Patel, J. Salmonson, and H. Scott, High Energy Density Phys. **6**, 171 (2010).
[11] S. Udrea, N. Shilkin, V. E. Fortov, D. H. H. Hoffmann, J. Jacoby, M. I. Kulish, V. Mintsev, P. Ni, D. Nikolaev, N. A. Tahir, and D. Varentsov, J. Phys. A **39**, 4743 (2006).
[12] V. N. Korobenko, A. D. Rakhel, A. I. Savvatimski, and V. E. Fortov, Phys. Rev. B **71**, 014208 (2005).
[13] A. N. Mostovych and Y. Chan, Phys. Rev. Lett. **79**, 5094 (1997).
[14] J. F. Benage, W. R. Shanahan, and M. S. Murillo, Phys. Rev. Lett. **83**, 2953 (1999).
[15] P. D. Desai, H. M. James, and C. Y. Ho, J. Phys. Chem. Ref. Data **13**, 1131 (1984).
[16] K. Y. Kim, B. Yellampalle, J. H. Glownia, A. J. Taylor, and G. Rodriguez, Phys. Rev. Lett. **100**, 135002 (2008).
[17] R. Brandt and G. Neuer, Int. J. Thermophys. **28**, 1429 (2007).
[18] G. R. Gathers, Int. J. Thermophys. **4**, 209 (1983).
[19] I. Krisch and H.-J. Kunze, Phys. Rev. E **58**, 6557 (1998).
[20] H. M. Milchberg, R. R. Freeman, S. C. Davey, and R. M. More, Phys. Rev. Lett. **61**, 2364 (1988).
[21] Z. Chen, B. Holst, S. E. Kirkwood, V. Sametoglu, M. Reid, Y. Y. Tsui, V. Recoules, and A. Ng, Phys. Rev. Lett. **110**, 135001 (2013).
[22] T. Ao, Y. Ping, K. Widmann, D. F. Price, E. Lee, H. Tam, P. T. Springer, and A. Ng, Phys. Rev. Lett. **96**, 055001 (2006).
[23] J. Clerouin, P. Noiret, V. Blottiau, B. Siberchicot, P. Renaudin, C. Blancard, G. Faussurier, B. Holst, and C. E. Starrett, Phys. Plasmas **19**, 082702 (2012).
[24] Y. T. Lee and R. M. More, Phys. Fluids **27**, 1273 (1984).
[25] G. Röpke, Phys. Rev. A **38**, 3001 (1988).
[26] H. Reinholz, R. Redmer, and S. Nagel, Phys. Rev. E **52**, 5368 (1995).
[27] M. W. C. Dharma-wardana and F. Perrot, Phys. Lett. A **163**, 223 (1992).
[28] S. Kuhlbrodt and R. Redmer, J. Phys. A **36**, 6027 (2003).
[29] G. Faussurier and C. Blancard, Phys. Rev. E **91**, 013105 (2015).
[30] C. E. Starrett, J. Clerouin, V. Recoules, J. D. Kress, L. A. Collins, and D. E. Hanson, Phys. Plasmas **19**, 102709 (2012).
[31] H. Reinholz, R. Redmer, G. Röpke, and A. Wierling, Phys. Rev. E **62**, 5648 (2000).
[32] M. P. Desjarlais, J. D. Kress, and L. A. Collins, Phys. Rev. E **66**, 025401 (2002).
[33] K.-U. Plagemann, P. Sperling, R. Thiele, M. P. Desjarlais, C. Fortmann, T. Döppner, H. J. Lee, S. H. Glenzer, and R. Redmer, New J. Phys. **14**, 055020 (2012).
[34] D. Alfè, M. Pozzo, and M. P. Desjarlais, Phys. Rev. B **85**, 024102 (2012).
[35] J. Clerouin, P. Renaudin, Y. Laudernet, P. Noiret, and M. P. Desjarlais, Phys. Rev. B **71**, 064203 (2005).
[36] A. L. Kritcher, P. Neumayer, J. Castor, T. Döppner, R. W. Falcone, O. L. Landen, H. J. Lee, R. W. Lee, E. C. Morse, A. Ng, S. Pollaine, D. Price, and S. H. Glenzer, Science **322**, 69 (2008).
[37] P. K. Patel, A. J. Mackinnon, M. H. Key, T. E. Cowan, M. E. Foord, M. Allen, D. F. Price, H. Ruhl, P. T. Springer, and R. Stephens, Phys. Rev. Lett. **91**, 125004 (2003).
[38] S. H. Glenzer, G. Gregori, R. W. Lee, F. J. Rogers, S. W. Pollaine, and O. L. Landen, Phys. Rev. Lett. **90**, 175002 (2003).
[39] T. Döppner, O. L. Landen, H. J. Lee, P. Neumayer, S. P. Regan, and S. H. Glenzer, High Energy Density Phys. **5**, 182 (2009).
[40] C. Fortmann, A. Wierling, and G. Röpke, Phys. Rev. E **81**, 026405 (2010).
[41] R. Fäustlin *et al.*, Phys. Rev. Lett. **104**, 125002 (2010).
[42] P. Emma *et al.*, Nat. Photonics **4**, 641 (2010).
[43] B. Lengeler, C. G. Schroer, M. Kuhlmann, B. Benner, T. F. Günzler, O. Kurapova, F. Zontone, A. Snigirev, and I. Snigireva, J. Phys. D **38**, A218 (2005).
[44] U. Zastrau, A. Woldegeorgis, E. Förster, R. Loetzsch, H. Marschner, and I. Uschmann, J. Instrum. **8**, P10006 (2013).
[45] U. Zastrau, L. B. Fletcher, E. Förster, E. C. Galtier, E. J. Gamboa, S. H. Glenzer, P. Heimann, H. Marschner, B. Nagler, A. Schropp, O. Wehrhan, and H. J. Lee, Rev. Sci. Instrum. **85**, 093106 (2014).
[46] H.-K. Chung, M. H. Chen, and R. W. Lee, High Energy Density Phys. **3**, 57 (2007).
[47] L. B. Fletcher, E. Galtier, P. Heimann, H.-J. Lee, B. Nagler, J. Welch, U. Zastrau, J. Hastings, and S. Glenzer, J. Instrum. **8**, C11014 (2013).
[48] J. Amann *et al.*, Nat. Photonics **6**, 693 (2012).
[49] N. D. Mermin, Phys. Rev. B **1**, 2362 (1970).
[50] G. Röpke, A. Selchow, A. Wierling, and H. Reinholz, Phys. Lett. A **260**, 365 (1999).
[51] See Supplemental Material http://link.aps.org/supplemental/10.1103/PhysRevLett.115.115001, which includes Refs. [52–54], for the (i) influence of plasma evolution, (ii) temperature determination, (iii) conductivity determination, and (iv) improved Born model.
[52] A. Selchow, G. Röpke, A. Wierling, H. Reinholz, T. Pschiwul, and G. Zwicknagel, Phys. Rev. E **64**, 056410 (2001).
[53] M. S. Wertheim, Phys. Rev. Lett. **10**, 321 (1963).
[54] G. Röpke, P. Schuck, Y. Funaki, H. Horiuchi, Z. Ren, A. Tohsaki, C. Xu, T. Yamada, and B. Zhou, Phys. Rev. C **90**, 034304 (2014).
[55] D. Pines and D. Bohm, Phys. Rev. **85**, 338 (1952).
[56] H. Reinholz, Ann. Phys. (Paris) **30**, 1 (2005).
[57] L. Spitzer and R. Härm, Phys. Rev. **89**, 977 (1953).
[58] H. Reinholz, G. Röpke, S. Rosmej, and R. Redmer, Phys. Rev. E **91**, 043105 (2015).
[59] M. R. Zaghloul, M. A. Bourham, and J. M. Doster, Phys. Lett. A **268**, 375 (2000).
[60] R. Bredow, T. Bornath, W.-D. Kraeft, M. W. C. Dharma-wardana, and R. Redmer, Contrib. Plasma Phys. **55**, 222 (2015).
[61] T. Schneider and E. Stoll, Phys. Kondens. Mater. **5**, 331 (1966).
[62] A. Ng, P. Celliers, A. Forsman, R. M. More, Y. T. Lee, F. Perrot, M. W. C. Dharma-wardana, and G. A. Rinker, Phys. Rev. Lett. **72**, 3351 (1994).